Supporting Information

Effect of substituents on FRET in rhodamine based chemosensors selective for Hg^{2+} ions

Siddhartha Pal,[a] Buddhadeb Sen,[a] Manjira Mukherjee,[a] Koushik Dhara,[b] Ennio Zangrando,[c] Sushil Kumar Mandal,[d] Anisur Rahman Khuda-Bukhsh,[d] and Pabitra Chattopadhyay*[a]

[a]*Department of Chemistry, Burdwan University, Golapbag, Burdwan, 713104, India,*

[b]*Department of Chemistry, Sambhu Nath College, Labpur, Birbhum 731303, West Bengal, India*

[c]*Dipartimento di Scienze Chimiche e Farmaceutiche, Via Licio Giorgieri 1, 34127 Trieste, Italy*
[d]*Molecular Biology and Genetics Laboratory, Department of Zoology, Kalyani University, India*

Corresponding author: pabitracc@yahoo.com

1. Materials and physical methods

1.1 General Procedures

High-purity HEPES, 4-methoxybenzaldehyde, 4-nitrobenzaldehyde and mercury(II) chloride were purchased from Sigma Aldrich (India) and rhodamine B from E. Merck, solvents used were spectroscopic grade. All metal salts were used as either their nitrate or their chloride salts. Other chemicals were of analytical reagent grade and used without further purification except when specified. Milli-Q, 18.2 MΩ cm^{-1} water was used throughout all experiments. A Shimadzu (model UV-1800) spectrophotometer was used for recording electronic spectra. FTIR spectra were recorded using Perkin Elmer FTIR model RX1 spectrometer preparing KBr disk. ^{1}HNMR spectrum of organic moiety was obtained on a Bruker Avance DPX 400 and 500 MHz spectrometer using DMSO-d_6 solution. Electrospray ionization (ESI) mass spectra were recorded on a Qtof Micro YA263 mass spectrometer. A Systronics digital pH meter (model 335) was used to measure the pH of the solution and the adjustment of pH was done using either 50 mM HCl or NaOH solution. Steady-state fluorescence emission and excitation spectra were recorded with a Perkin Elmer LS 55 spectrofluorimeter. Time-resolved fluorescence lifetime measurements were performed using a HORIBA JOBIN Yvon picosecond pulsed diode laser-based time-correlated single-photon counting (TCSPC) spectrometer from IBH (UK) at λ_{ex}= 340 nm and 560 nm, and MCP-PMT as a detector. Emission from the sample was collected at a right angle to the direction of the excitation beam maintaining magic angle polarization (54.71). The full width at half-maximum (FWHM) of the instrument response function was 250 ps, and the resolution was 28.6 ps per channel. Data were fitted to multiexponential functions after deconvolution of the instrument response function by an iterative reconvolution technique using IBH DAS 6.2 data analysis software in which reduced w2 and weighted residuals serve as parameters for goodness of fit.

1.2 General method of UV-vis and fluorescence titration

Path length of the cells used for absorption and emission studies was 1 cm. For UV-vis and fluorescence titrations, stock solution of $\mathbf{L^1}$and $\mathbf{L^2}$ was prepared in HEPES buffer (1 mM, pH 7.4; DMSO/water: 1/9, v/v) at 25 °C. Working solutions of $\mathbf{L^1}$/ $\mathbf{L^2}$ and Hg^{2+} were prepared from their respective stock solutions. Fluorescence measurements were performed using 15 nm x 5 nm

slit width. All the fluorescence and absorbance spectra were taken after 15 minutes of mixing of Hg^{2+} and **L^1/ L^2**.

1.3 Job's plot from fluorescence experiments

A series of solutions containing **L^1/ L^2** and $HgCl_2$ were prepared such that the total concentration of Hg^{2+} and **L^1/ L^2** remained constant (10 μM) in all the sets. The mole fractions of Hg^{2+} ions with respect to **L^1**and **L^2** were varied from 0.1 to 0.75. The fluorescence intensity (**L^1**) at 585 nm was plotted against mole fraction [Hg^{2+}] and in case of **L^2** the fluorescence intensity at 584 nm *versus* mole fraction [Hg^{2+}].

2. Preparation

2.1. Synthesis of the probes (**L^1**and **L^2**)

The organic moieties **(**$L^1$and **L^2**) were prepared following a common procedure as stated below. At first, rhodamine B was converted to rhodamine B-hydrazide by a similar procedure to that reported procedure[1]. Then this rhodamine B-hydrazide was allowed to react with corresponding *para*-substituted to get **L^1**and **L^2 (***viz.* Scheme S1**).**

Synthesis of L^1. *4-Methoxybenzaldehyde* (136 mg, 1.0 mmol) was dissolved in ethanol and was added to the ethanolic solution rhodamine-B hydrazide (456 mg, 1.0 mmol) with stirring. Then the resulting solution was reflux for 6 h. Evaporated to a small volume and cooled, white colored mass precipitated out which was filtered out and then recrystallized from pure acetonitrile. Single crystals were obtained from this solution, one of which was selected for doing the crystallographic study.

$C_{36}H_{38}N_4O_3$: m.p.: 190 ^oC. IR (KBr, cm^{-1}): $\nu_{OH,}$ 3448; $\nu_{NH,}$ 3080; $\nu_{C=C(aromatic)}$, 2972; $\nu_{C=O}$, 1689; $\nu_{CH=N}$, 1617. ^1H NMR (δ, ppm in dmso-d_6): 8.86 (s, 1H, CH=N); 7.87 (d, 1H); 7.58-7.54 (m, 2H); 7.36 (d, 2H); 7.08(d, 1H); 6.90(d, 2H); 6.42-6.37(m, 4H); 6.32-6.29 (m, 2H); 3.72(s, 3H, OMe); 3.28(q, 8H, $4CH_2$); 1.05(t, 12H, $4CH_3$). ESI-MS (in ethanol): $[M + H]^+$, m/z, 575.1497 (100 %) (calcd.: m/z, 575.29; where M = molecular weight of **L^1**], $[M + Na]^+$, m/z, 597.1536 (8 %). Yield: 86%.

Synthesis of L^2. *4-Nitrobenzaldehyde* (151 mg, 1.0 mmol) was dissolved in ethanol and was added to the ethanolic solution rhodamine-B hydrazide (456 mg, 0.6 mmol) with stirring. Then

the resulting solution was reflux for 4 h. Evaporated to a small volume and cooled, light yellow colored solid precipitated out which was filtered out. The crystalline product was collected from the solution in DMF-acetonitrile, and the single crystals for X-ray diffraction were obtained from this solution on slow evaporation. .

$C_{35}H_{35}N_5O_4$: m.p. 238 ^oC. IR (KBr, cm^{-1}): $\nu_{OH,}$ 3434; $\nu_{NH,}$ 3081; $\nu_{C=O}$, 1697; $\nu_{CH=N}$, 1610; ν_{NO2}, 1427. ^1H NMR (400 MHz, dmso-d6): 8.95 (s, 1H, CH=N); 8.19-8.14 (m, 2H); 7.93 (d, 1H); 7.66-7.56 (m, 4H); 7.12(d, 1H); 6.44-6.39(m, 4H); 6.34-6.31(m, 2H); 3.28(q, 8H, $4CH_2$); 1.05(t, 12H, $4CH_3$). ESI-MS (in acetonitrile): $[M + H]^+$, m/z, 590.1824 (100 %) (calcd.: m/z, 589.27; where M = molecular weight of **L**^{2}]. Yield: 86%.

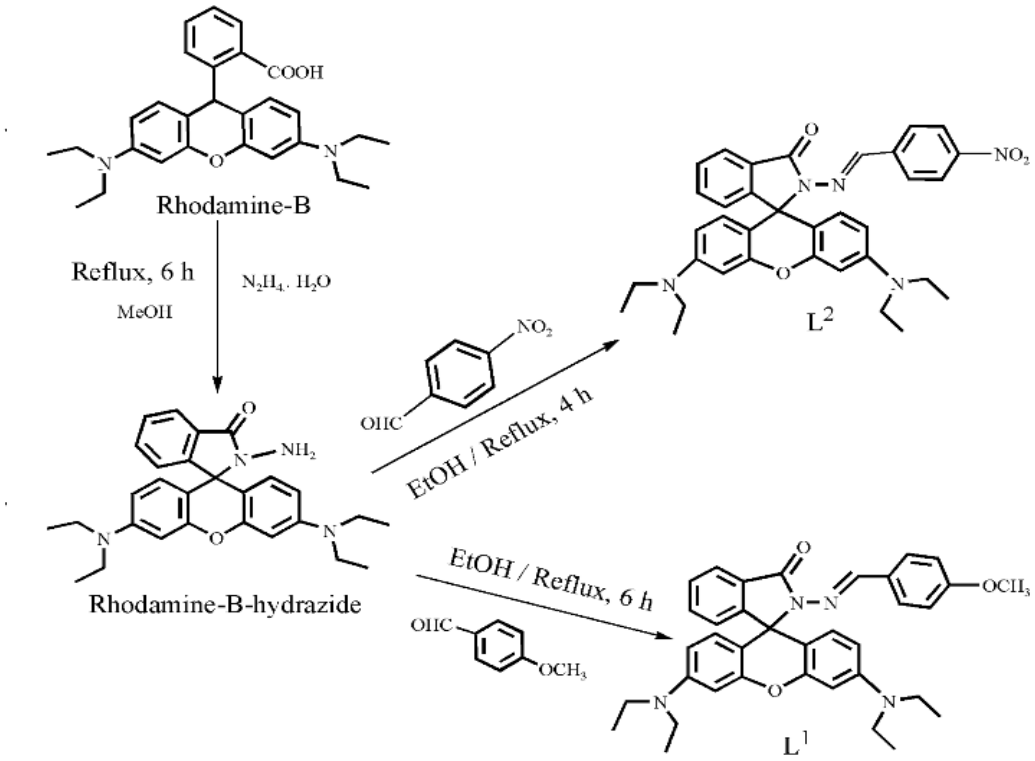

Scheme S1. Synthetic procedure of the probes, **L**^{1}and **L**^{2}.

2.2 Synthesis of L-Hg species as [Hg(L)Cl_2]

To a 10.0 mL ethanol solution of **L^1/ L^2** (0.01 mmol), a solution of mercury(II) chloride was added dropwise and stirred for 4 h. Solvent was removed using a rotary evaporator, while a blood red precipitate was obtained for L^1 and deep orange precipitate was obtained for L^2 (Scheme-S2).

[Hg(L^1)Cl_2]: $C_{36}H_{38}Cl_2HgN_4O_3$: Anal. Found: C, 51.10; H, 4.53; N, 6.62. Calc.: C, 50.35; H, 4.42; N, 6.21; Hg, 22.99. ^{1}H NMR (400 MHz, DMSO-d_6): ^{1}H NMR (δ, ppm in dmso-d_6): 8.92 (s, 1H, CH=N); 7.89 (d, 1H); 7.60-7.56 (m, 2H); 7.38 (d, 2H); 7.09(d, 1H); 6.91(d, 2H); 6.43-6.37(m, 4H); 6.33-6.30 (m, 2H); 3.75(s, 3H, OMe); 3.30(q, 8H, 4CH_2); 1.07(t, 12H, 4CH_3). ESI-MS in methanol: $[M]^+$, m/z, 845.9515 (obsd. with 16 % abundance) (Calc.: m/z, 846.20; where M = [Hg(L_1)Cl_2]; Yield : 67-70%.

[Hg(L^2)Cl_2]: $C_{35}H_{35}Cl_2HgN_5O_4$: C, 48.81; H, 4.10; N, 8.13. Calc.: C, 48.19; H, 4.01; N, 7.98. ^{1}H NMR (400 MHz, dmso-d6): 8.99 (s, 1H, CH=N); 8.20-8.15 (m, 2H); 7.94 (d, 1H); 7.68-7.58 (m, 4H); 7.15(d, 1H); 6.45-6.40(m, 4H); 6.35-6.32(m, 2H); 3.30(q, 8H, 4CH_2); 1.08(t, 12H, 4CH_3). ESI-MS in methanol: $[M]^+$, m/z, 861.4561 (obsd. with 14 % abundance) (Calc.: m/z, 861.18; where M = [Hg(L_2)Cl_2]; Yield : 48-55%.

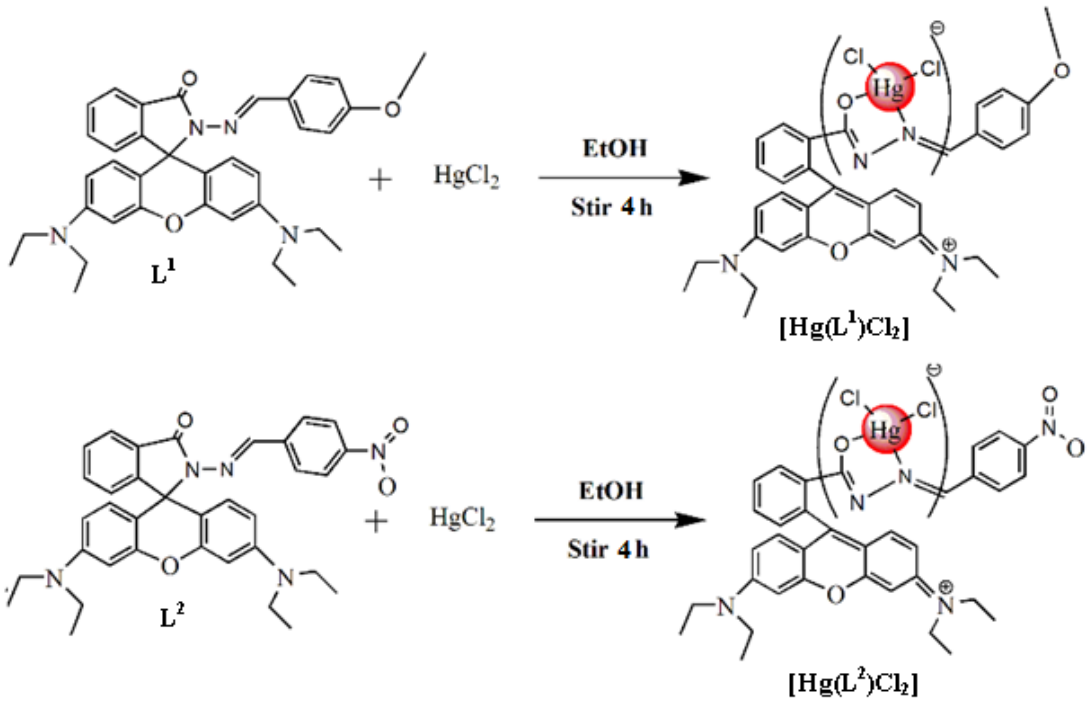

Scheme S2. Schematic representation of synthesis of the **L-Hg** complexes of **L^1** and **L^2**

3. Structural analyses of L^1 and L^2

X-ray single crystal data were collected using Mo-K_α (λ = 0.7107 Å) radiation on a SMART APEX II diffractometer equipped with CCD area detector. Data collection, data reduction, structure solution/refinement were carried out using the software package of SMART APEX II. Crystallographic data and selected bond lengths and bond angles are tabulated in Table S3 and S4. Details are available in the CCDC nos. 961462 and 961461 for crystal data of $\mathbf{L^1}$ and $\mathbf{L^2}$, respectively. ·

4. Spectral Characteristics

4.1 Emission study

Organic moiety ($\mathbf{L^1}$) shows emission spectrum at 585 nm in HEPES buffer (1 mM, pH 7.4; DMSO/water: 1/9, v/v) at 25 °C excited at 340 nm considering the absorption at 335 nm. Similarly L^2 shows emission spectrum at 584 nm in HEPES buffer (1 mM, pH 7.4; DMSO/water: 1/9, v/v) at 25 °C excited at 555 nm considering the absorption at 555 nm Fluorescence quantum yields (Φ) were estimated by integrating the area under the fluorescence curves with the equation:

$$\Phi_{sample} = \Phi_{ref} \times \frac{OD_{ref} \times A_{sample} \times \eta^2_{sample}}{OD_{sample} \times A_{ref} \times \eta^2_{ref}}$$

where A is the area under the fluorescence spectral curve and OD is optical density of the compound at the excitation wavelength, 550 nm, η is the refractive index of the solvent used. The standard used for the measurement of fluorescence quantum yield was rhodamine-B (Φ = 0.7 in ethanol).

In case of L^1 the fluorescence quantum yield has been calculated in absence and presence of Hg^{2+} ion and from this measurement it is clear that the fluorescence quantum yield increases more than 7 times (at λ= 585 nm) upon addition of 3.0 equivalent of Hg^{2+}, where in case of $\mathbf{L^2}$ it is 5 times (at λ= 584 nm) upon addition of 3.0 equivalent of Hg^{2+}. From Job's plot analysis it is revealed that maximum emission shows at 1:1 ratio ($\mathbf{L^1}$/ $\mathbf{L^2}$:Hg^{2+}). These data indicate that the

complex species in solution should form 1:1 complex with Hg^{2+} clear from the mass spectrum and NMR. The binding constant value was determined from the emission intensity data following the modified Benesi-Hildebrand equation.

$$\mathbf{1/(F_x-F_0)=1/(F_{max}-F_0)+(1/K\,[C])(1/(F_{max}-F_0)}$$

where F_0, F_x, and F_∞ are the emission intensities of organic moiety considered in the absence of Hg^{2+} ion, at an intermediate Hg^{2+} concentration, and at a concentration of complete interaction, respectively, and where K is the association constant and [C] is the Hg^{2+} concentration. K values (5.55×10^5 L.mol^{-1} for **L^1** and 1.38×10^5 L.mol^{-1} for **L^2**) were calculated from the intercept /slope using the plot of $(F_\infty - F_0)/(F_x - F_0)$ against $[C]^{-1}$. From these values, it is reflected that the higher binding constant of **L^1** is the indication of stronger binding affinity towards the Hg^{2+} ion than that of **L^2**.

Spectral properties of both (L^1 and L^2) probes are very good in terms selectivity and sensitivity towards Hg^{2+} ions by naked eye using UV-Vis and fluorescence study (**Figs. S31 to S36**).

4.2 Calculation of the energy transfer based on the Förster equation:[2-3]

$$\mathbf{E= R_0^6/(R_0^6 + R^6)}$$

Where R_0 is the Förster distance; R is the distance between energy donor dye and energy acceptor dye. The Förster critical distance (R_0) of **L^1** was calculated to be 48.6 Å by the simplified equation below:

$$\mathbf{R_0 = 0.211\,[\,k^2 n^{-4} \Phi_D J_{DA}\,]^{1/6} = 0.211\,[\,}\boldsymbol{k^2 n^{-4} \Phi_D \int_0^\infty I_D(\lambda)\,\varepsilon_A(\lambda)\,\lambda^4\,d\lambda}\mathbf{\,]^{1/6}} \quad \textbf{(in Å)}$$

Where n is the refractive index (n = 1.33 in water)[4]; Φ_D is the quantum yield of the donor; k denotes the average squared orientational part of a dipole-dipole interaction, typically k^2 =2/3;[3] J_{DA} expresses the degree of spectral overlap between the donor emission and the acceptor absorption; $I_D(\lambda)$ is the normalized fluorescence spectra of the donor; $\varepsilon_A(\lambda)$ is the molar absorption coefficient of the acceptor.

5. Theoretical Calculation

To clarify the understanding of the configurations and the mechanism of process of enhancement of fluorescence, DFT calculations of the excited state character of the probes (L^1 and L^2) and their L-Hg complexes were performed using **Gaussian-09** software over a **Red Hat**

Linux IBM cluster. Molecular level interactions have also been studied using density functional theory (DFT) with the **B3LYP/6-31G (d)** functional model and basis set.

6. Preparation of cell and in vitro cellular imaging with L^1/L^2

Human cervical cancer cell, HeLa cell line was purchased from National Center for Cell Science (NCCS), Pune, India and was used throughout the study. Cell were cultured in Dulbecco's modified Eagle's medium (DMEM, Gibco BRL) supplemented with 10% FBS (Gibco BRL), and 1% antibiotic mixture containing penicillin, streptomycin and neomycin (PSN, Gibco BRL), at 37 °C in a humidified incubator with 5% CO_2. For experimental study, cells were grown to 80-90 % confluence, harvested with 0.025 % trypsin (Gibco BRL) and 0.52 mM EDTA (Gibco BRL) in PBS (phosphate-buffered saline, Sigma Diagnostics) and plated at desire cell concentration and allowed to re-equilibrate for 24h before any treatment. Cells were rinsed with PBS and incubated with DMEM-containing $\mathbf{L^1/L^2}$ (10 μM, 1% DMSO) for 30 min at 25 °C. All experiments were conducted in DMEM containing 10% FBS and 1% PSN antibiotic. The imaging system was composed of a fluorescence microscope (ZEISS Axioskop 2 plus) with an objective lens [10×].

7 Cell cytotoxicity assay

To test the cytotoxicity of $\mathbf{L^1/L^2}$, MTT [3-(4,5-dimethyl-thiazol-2-yl)-2,S-diphenyl tetrazolium bromide] assay was performed by the procedure described earlier.[7] After treatments of the probe (1, 10, 20, 50, and 100 μM), 10 μl of MTT solution (10mg/ml PBS) was added in each well of a 96-well culture plate and incubated continuously at 25 °C for 6 h. All mediums were removed from wells and replaced with 100 μl of acidic isopropanol. The intracellular formazan crystals (blue-violet) formed were solubilized with 0.04 N acidic isopropanol and the absorbance of the solution was measured at 595 nm wavelength with a microplate reader. Values are means ± S.D. of three independent experiments. The cell cytotoxicity was calculated as percent cell cytotoxicity = 100% cell viability.

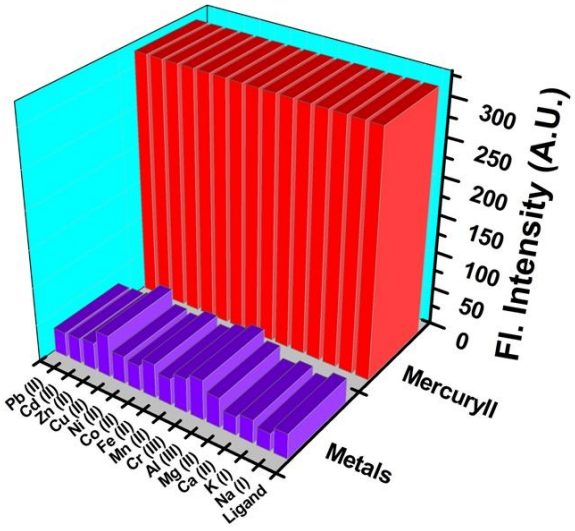

Fig.S1. Change of relative fluorescence intensity profile of $\mathbf{L^1}$ in presence of different ions in DMSO-Water (1:9, v/v) at 25 °C (λ_{ex} = 340 nm)

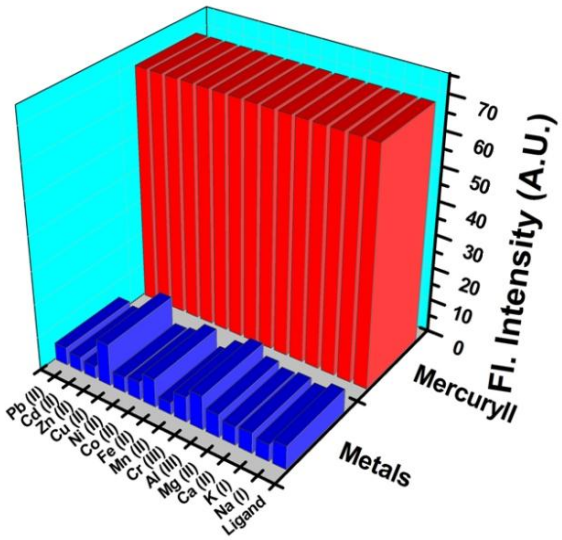

Fig.S2. Change of relative fluorescence intensity profile of $\mathbf{L^2}$ in presence of different ions in DMSO-Water (1:9, v/v) at 25 °C (λ_{ex} = 555nm)

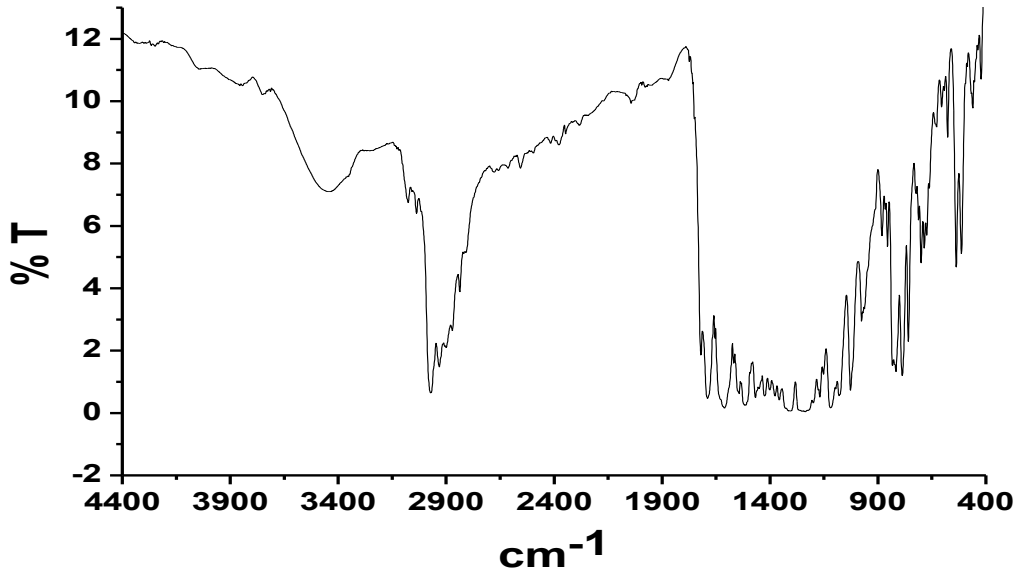

Fig.S3 FTIR spectrum of $\mathbf{L^1}$

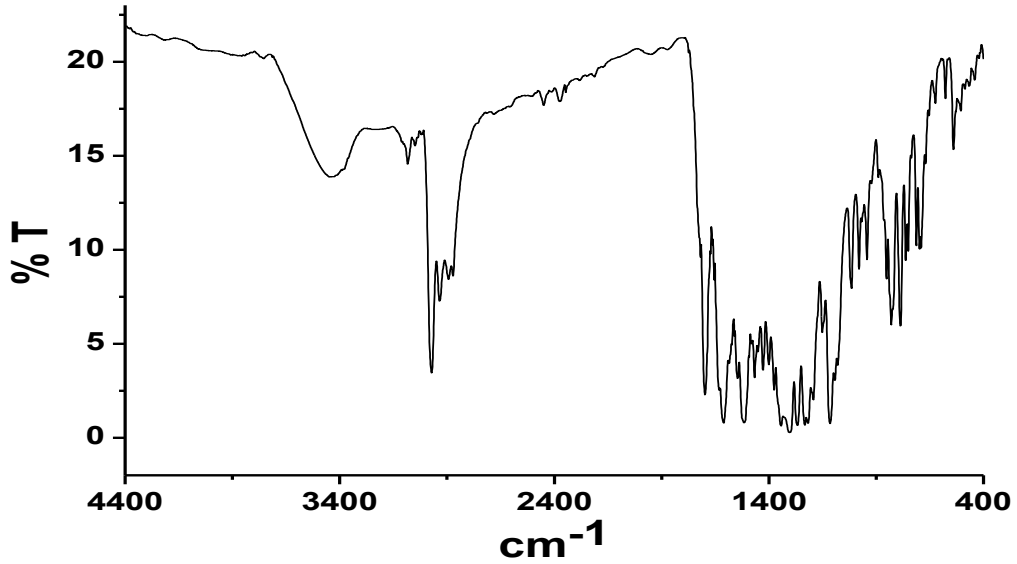

Fig.S4 FTIR spectrum of $\mathbf{L^2}$

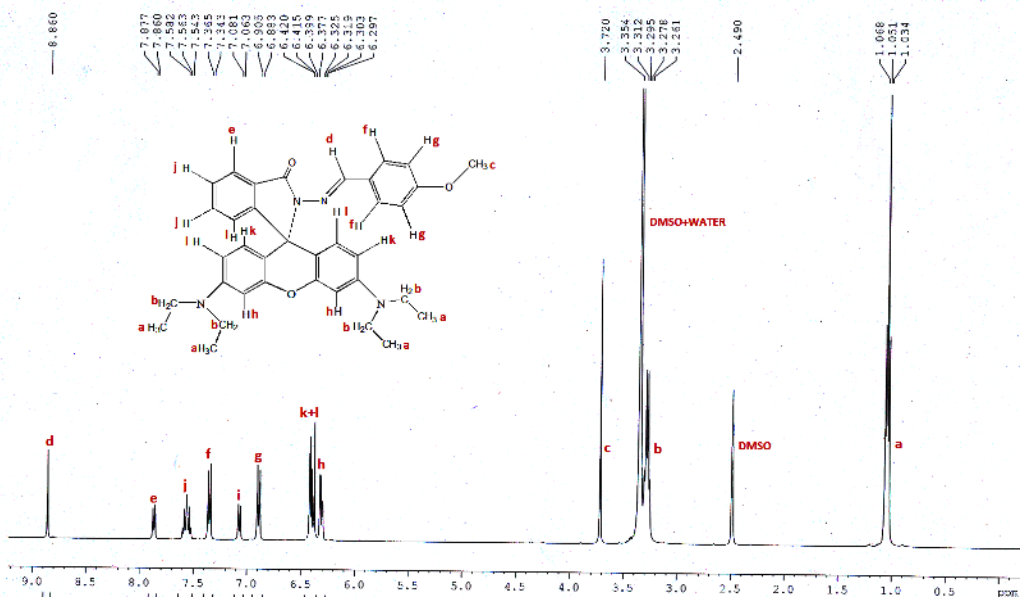

Fig.S5 ^{1}H NMR of the probe (**L**^{1}) in dmso-d$_6$

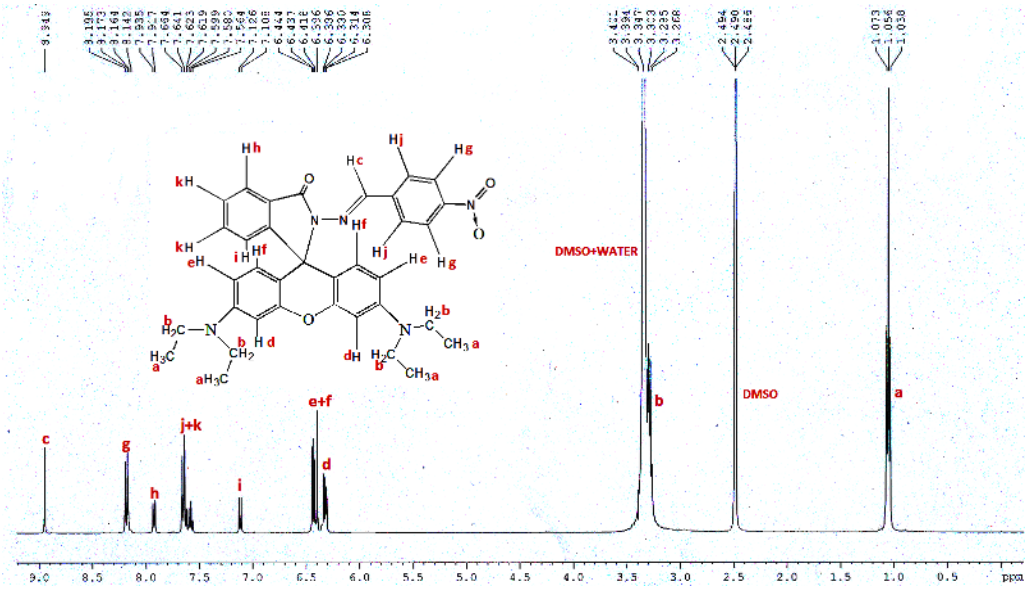

Fig.S6 ^{1}H NMR of the probe (**L**^{2}) in dmso-d$_6$

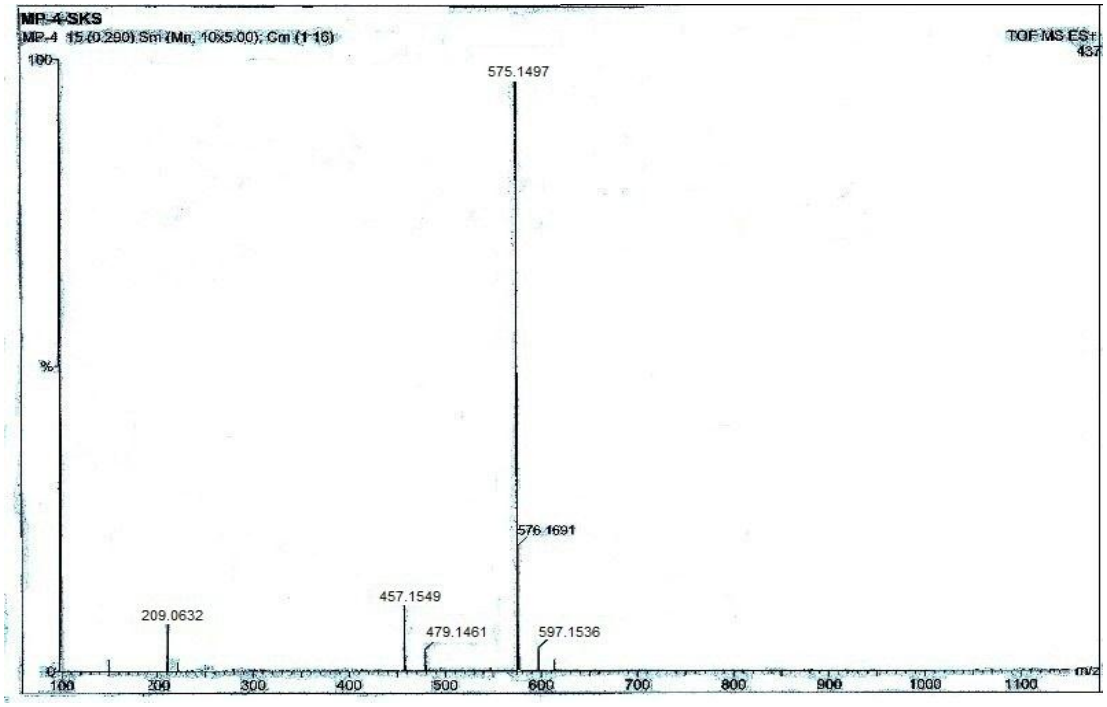

Fig.S7 ESI-MS of the probe ($\mathbf{L^1}$) in ethanol

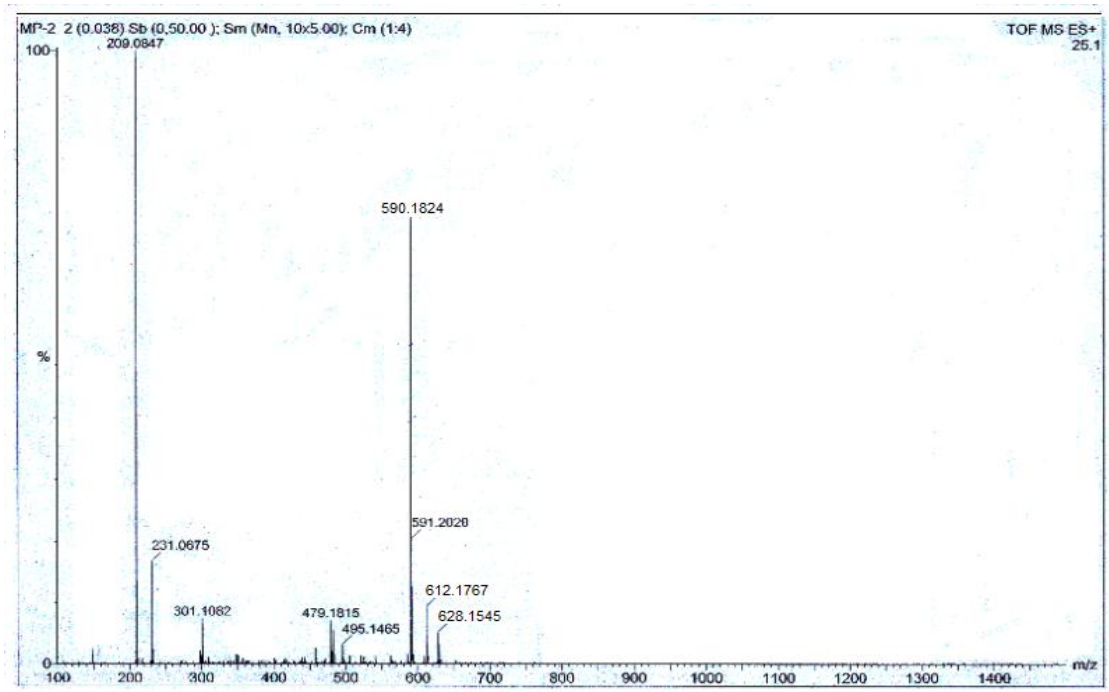

Fig.S8 ESI-MS of the probe ($\mathbf{L^2}$) in acetonitrile

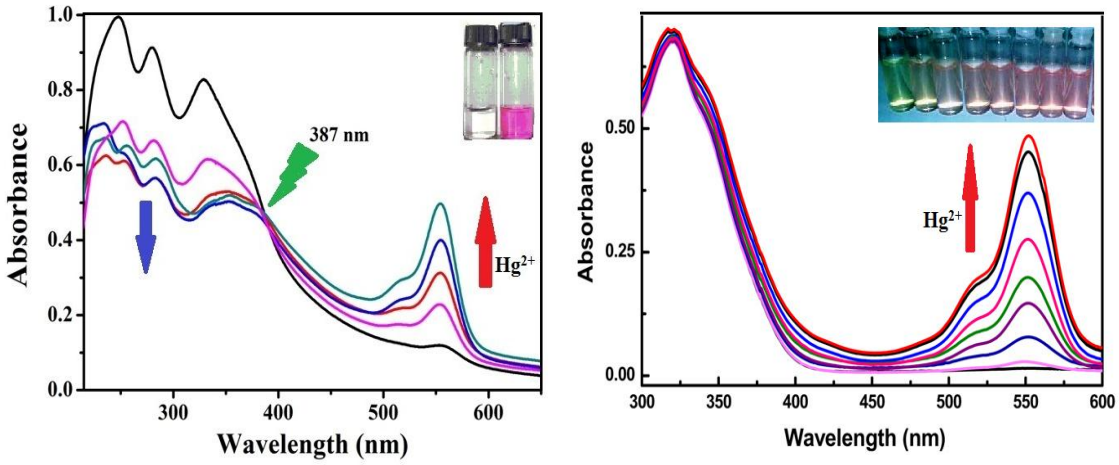

(a) **(b)**

Fig.S9 UV-Vis titration spectra of (a) **L**^{1} (10 μM) and (b) **L**^{2} upon incremental addition of Hg^{2+} ions (0-30 μM) in DMSO/water (1:9 v/v); in case of **L**^{1} an isobestic point at 387 nm but in case of **L**^{2} no isobestic point

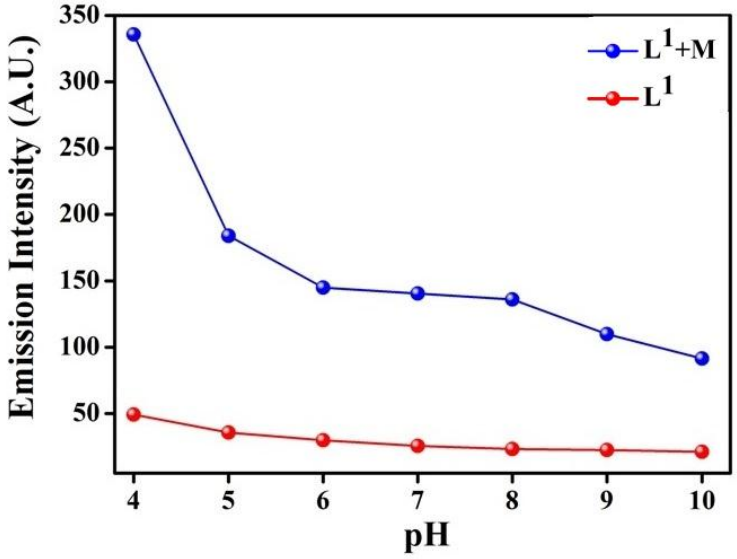

Fig. S10 Effect of pH of L^{1} in absence of Hg^{2+} (A) and in presence of Hg^{2+}(B)

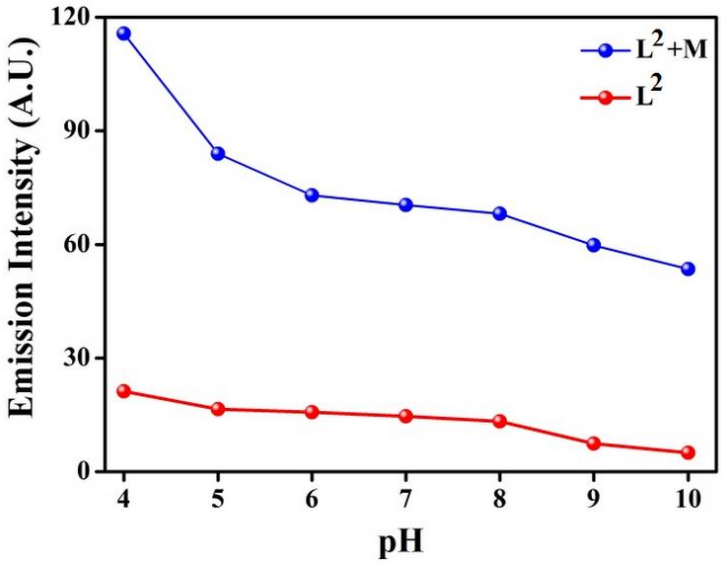

Fig. S11 Effect of pH of L^2 in absence of Hg^{2+} (A) and in presence of Hg^{2+}(B)

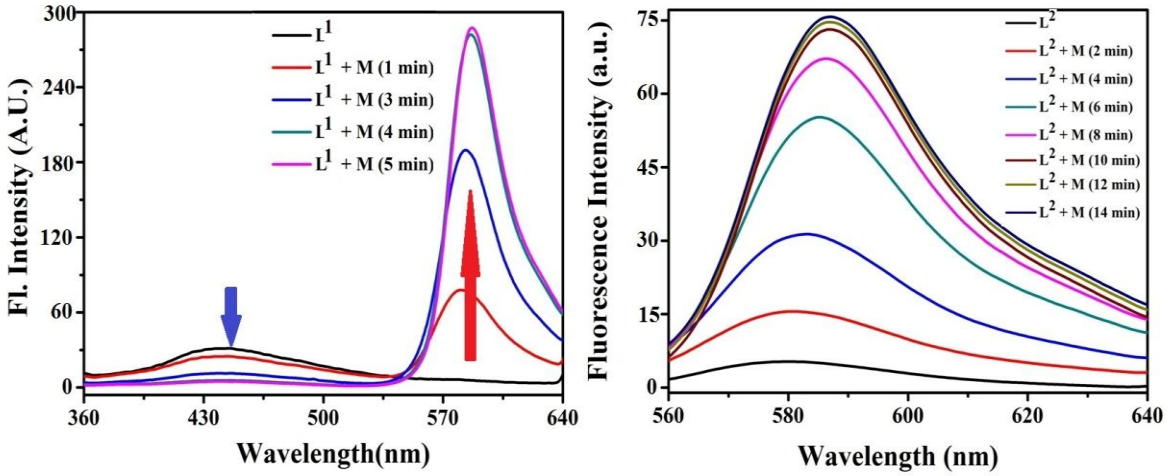

Fig.S12. The kinetic study of the fluorescence data

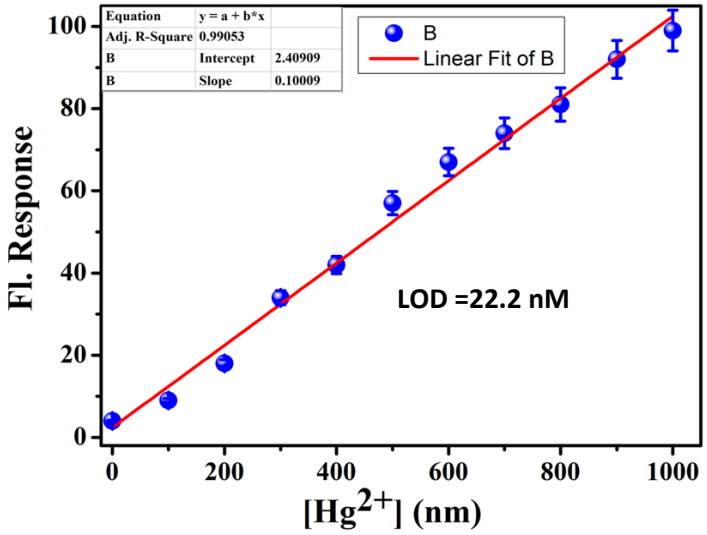

Fig.S13 calibration curve for the nanomolar range, with error bars for calculating the LOD of Hg^{2+} by $\mathbf{L^1}$ in HEPES buffer (1 mM, pH 7.4; DMSO/water: 1/9, v/v) at 25 °C

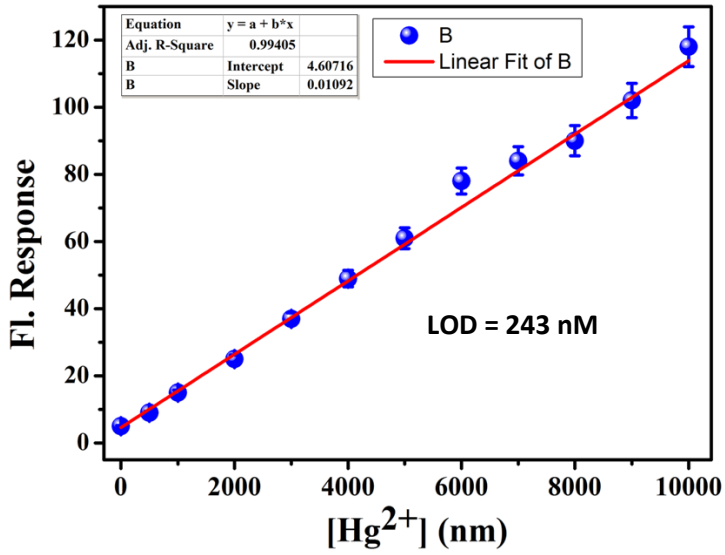

Fig.S14 calibration curve for the nanomolar range, with error bars for calculating the LOD of Hg^{2+} by $\mathbf{L^2}$ in HEPES buffer (1 mM, pH 7.4; DMSO/water: 1/9, v/v) at 25 °C

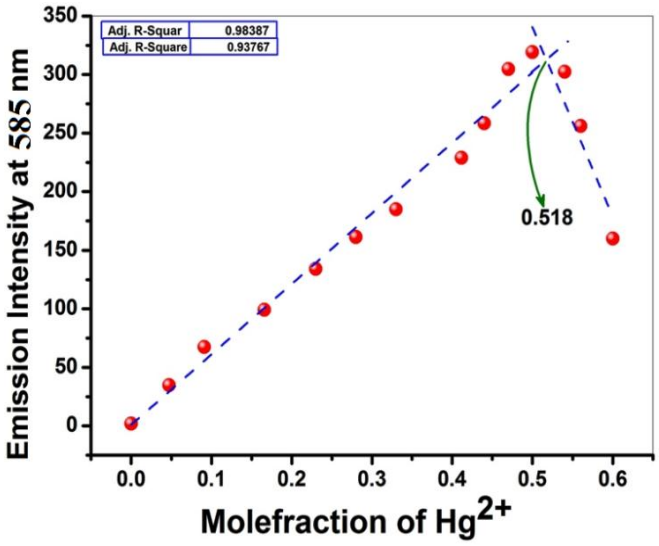

Fig.S15 Job's plot analysis from emission intensity showing maximum emission at 1:1 ratio [$\mathbf{L^1}$: Hg^{2+}]

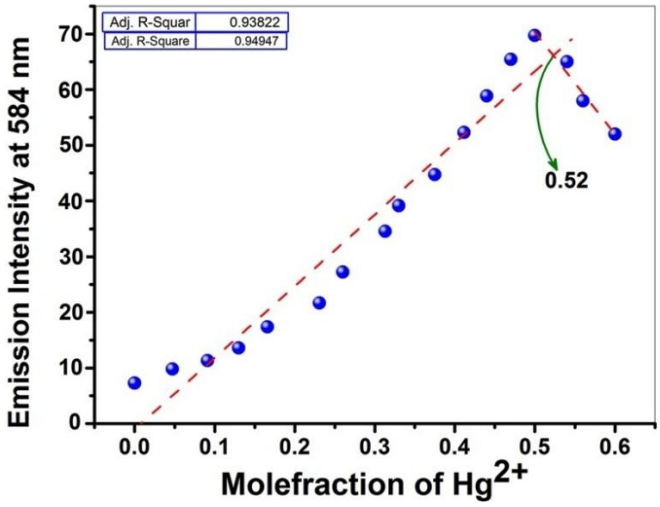

Fig.S16 Job's plot analysis from emission intensity showing maximum emission at 1:1 ratio [$\mathbf{L^2}$: Hg^{2+}]

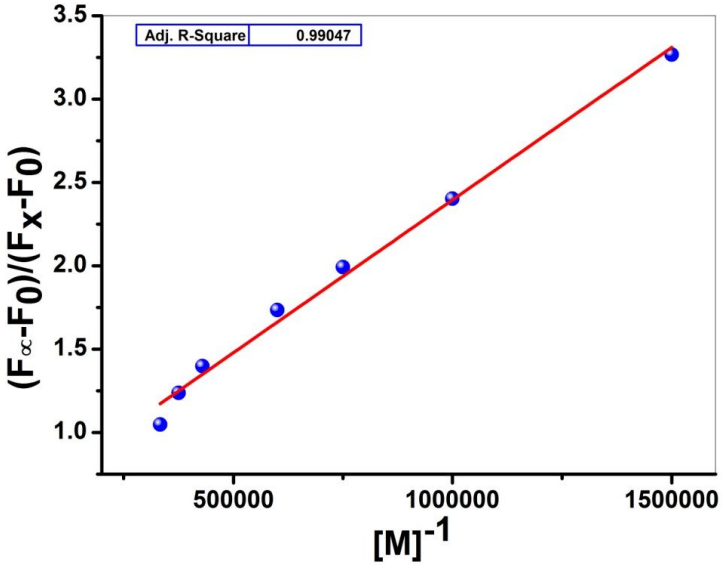

Fig.S17 Binding constant (K) value 5.55 X 10^5 M^{-1} determined from the interactions of $\mathbf{L^1}$ with Hg^{2+}

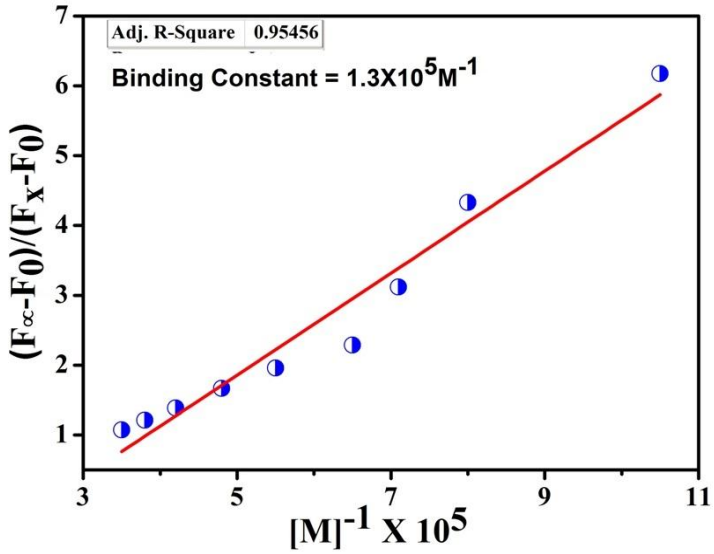

Fig.S18 Binding constant (K) value 1.38 X 10^5M^{-1} determined from the interactions of $\mathbf{L^2}$ with Hg^{2+}

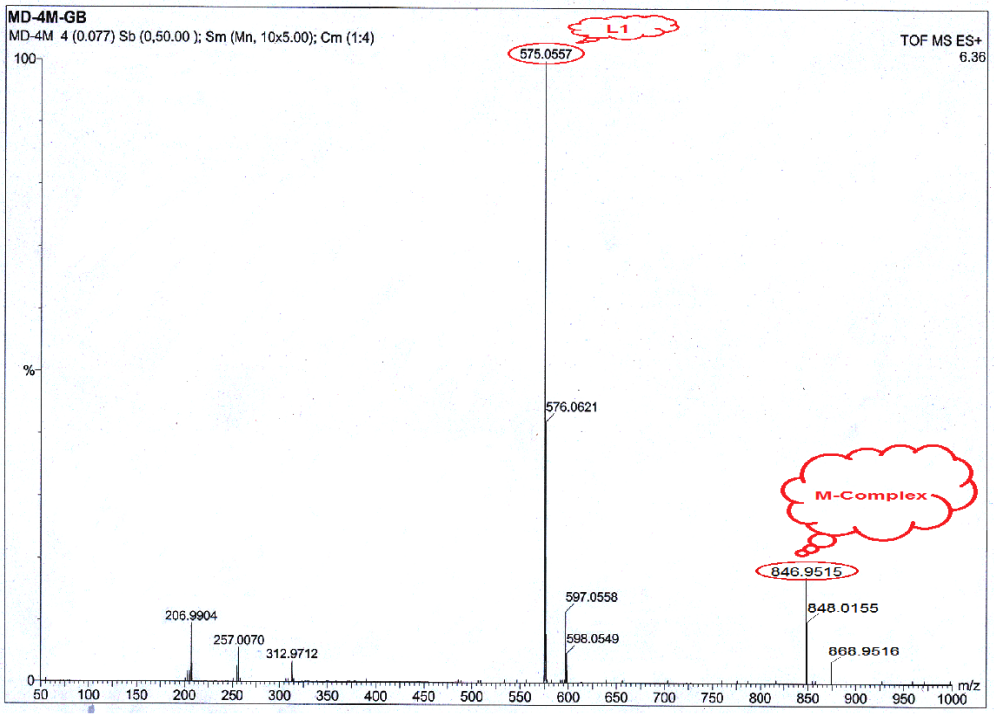

Fig.S19 ESI-MS of **L^1-Hg** in methanol

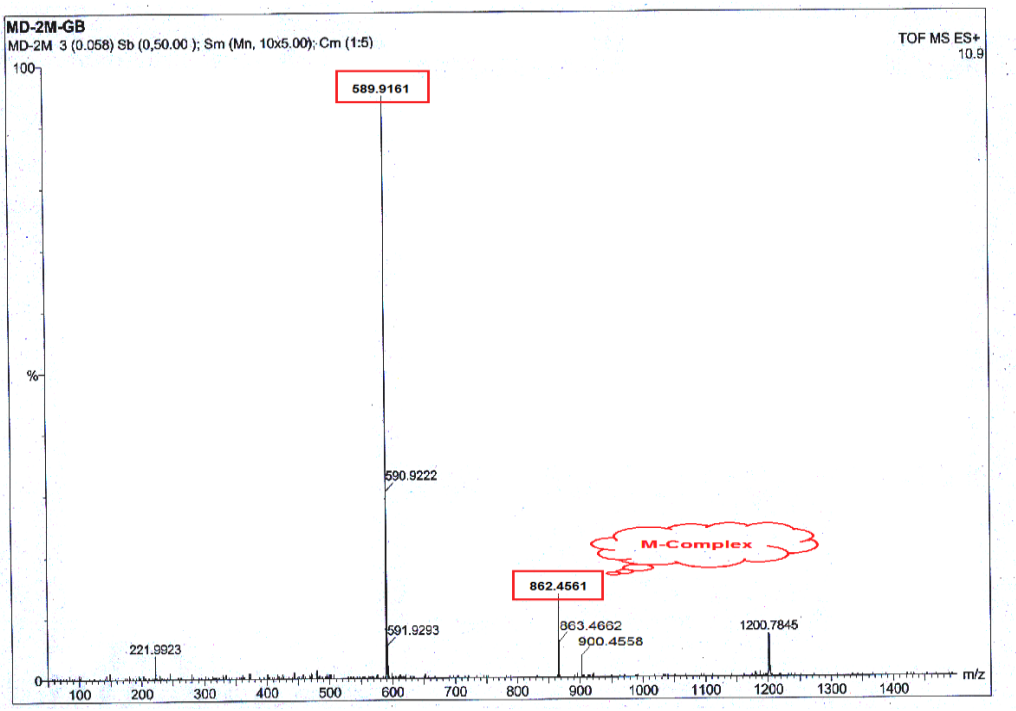

Fig.S20 ESI-MS of **L^2-Hg** in methanol

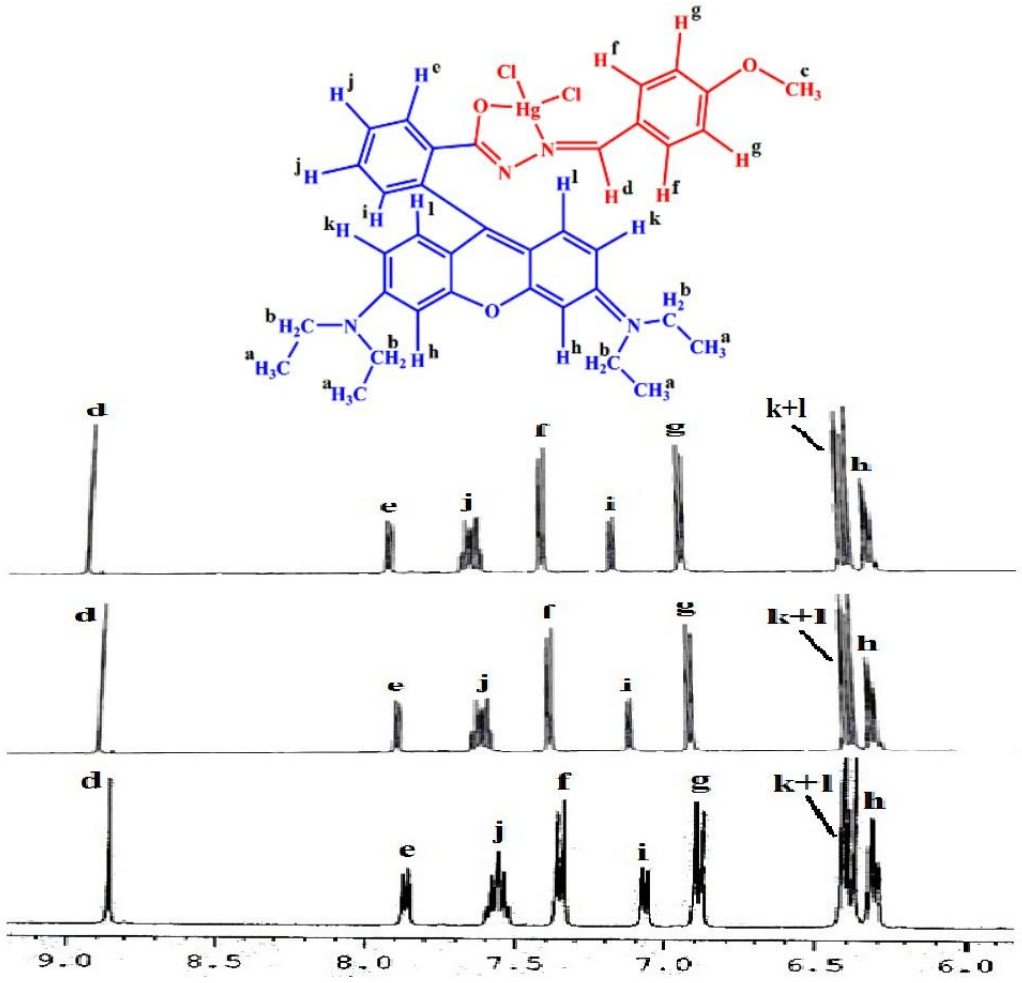

Fig.S21 Partial ^{1}H NMR spectra for $\mathbf{L^1}$ (5 mM) in presence of varying [Hg^{2+}] (a) 0, (b) 2.0 and (c) 5 mM [Hg^{2+}] ions of in DMSO-d_6.

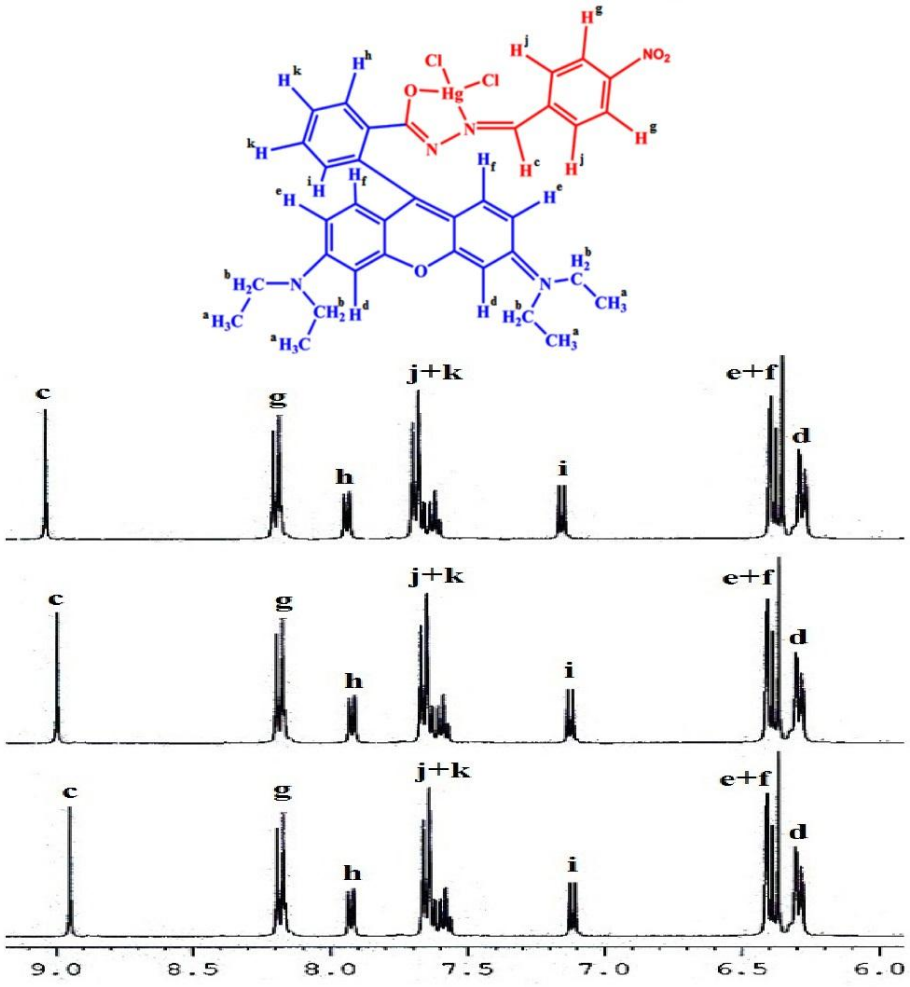

Fig.S22 Partial ^{1}H NMR spectra for **L^{2}** (5 mM) in presence of varying [Hg^{2+}] (a) 0, (b) 2.0 and (c) 5 mM [Hg^{2+}] ions of in DMSO-d_6.

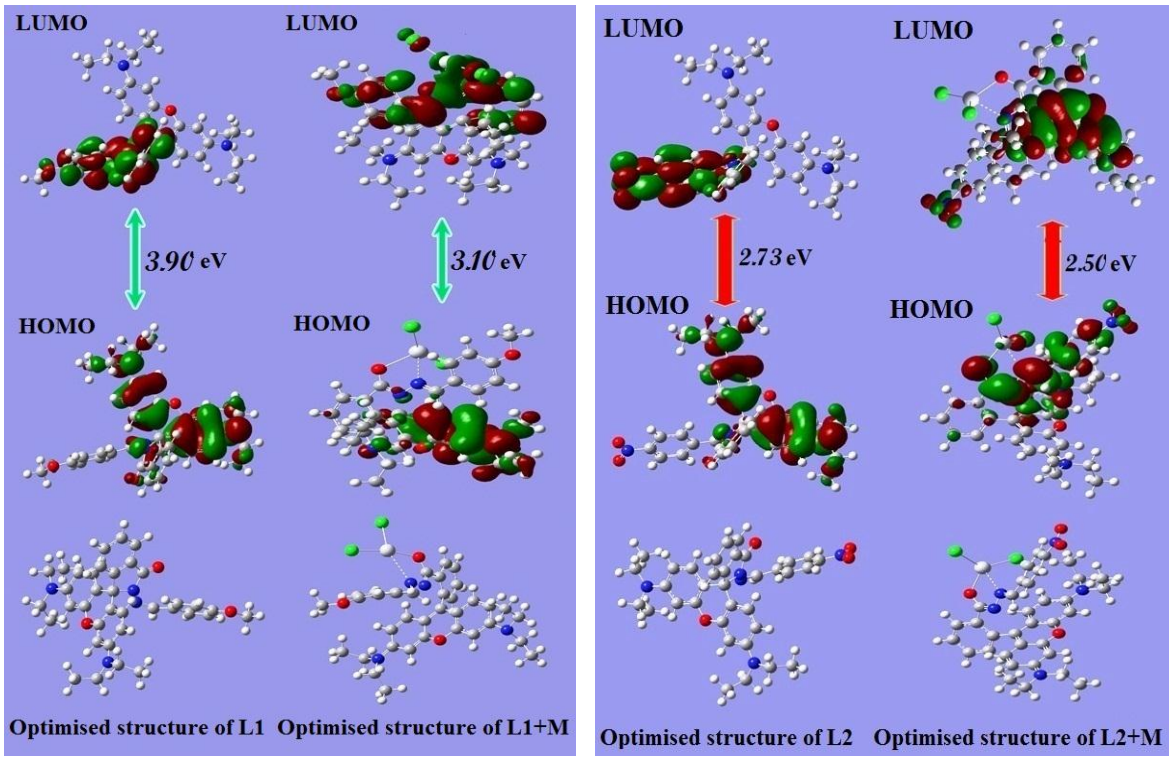

Fig. S23. Optimised structures of (a) $\mathbf{L^1}$ and $\mathbf{L^1}$**-Hg**; (b) $\mathbf{L^2}$ and $\mathbf{L^2}$**-Hg** species

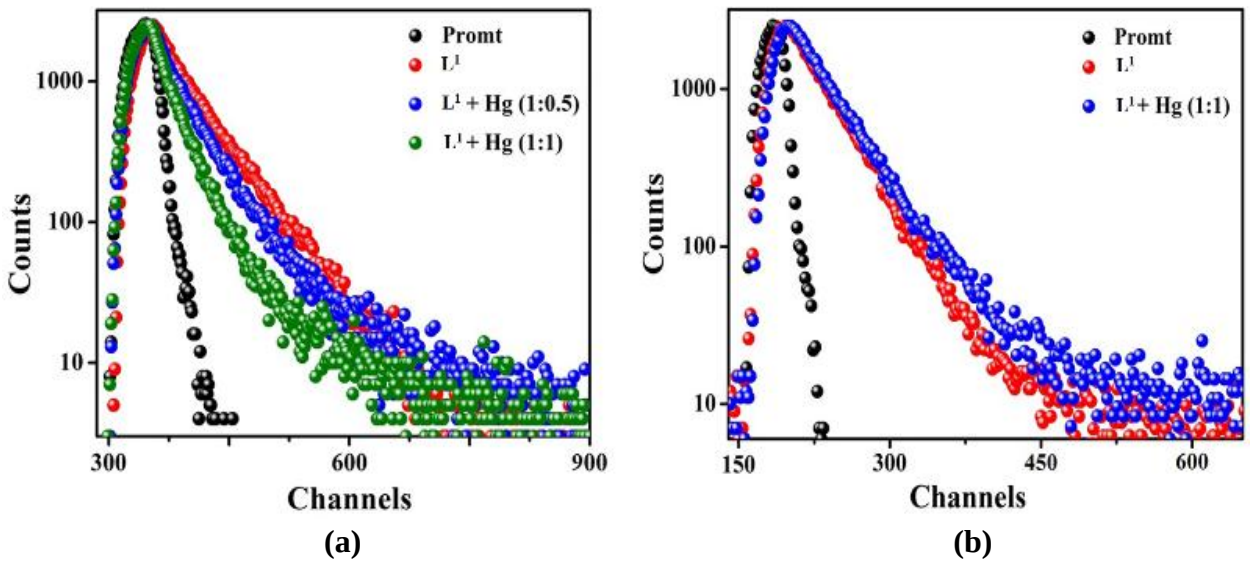

Fig. S24 Fluorescence life time experiment of $\mathbf{L^1}$ (a) at 440 nm (data related to life time in Table S3A) and (b) at 585 nm (data related to life time in Table S3B)

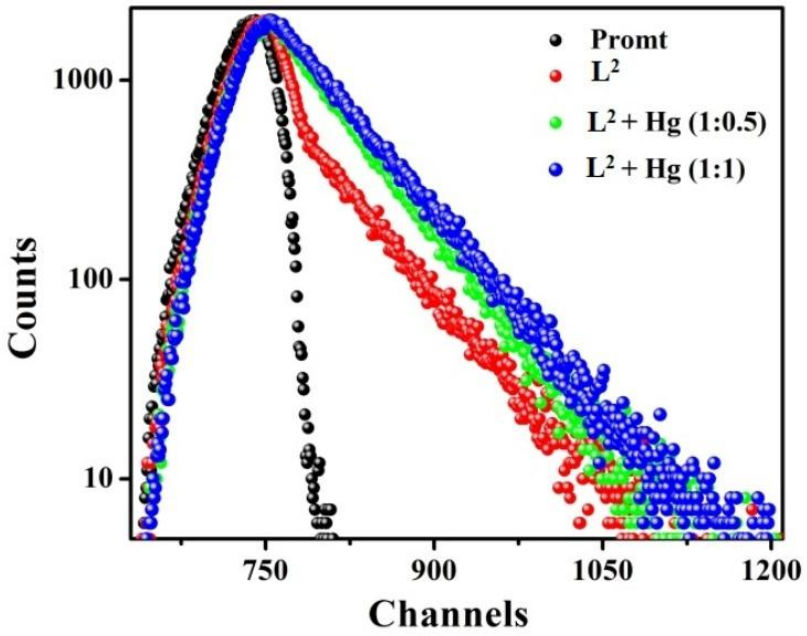

Fig. S25 Measurement of fluorescence life times of **L²** at 584 nm (data related to life time in Table S4)

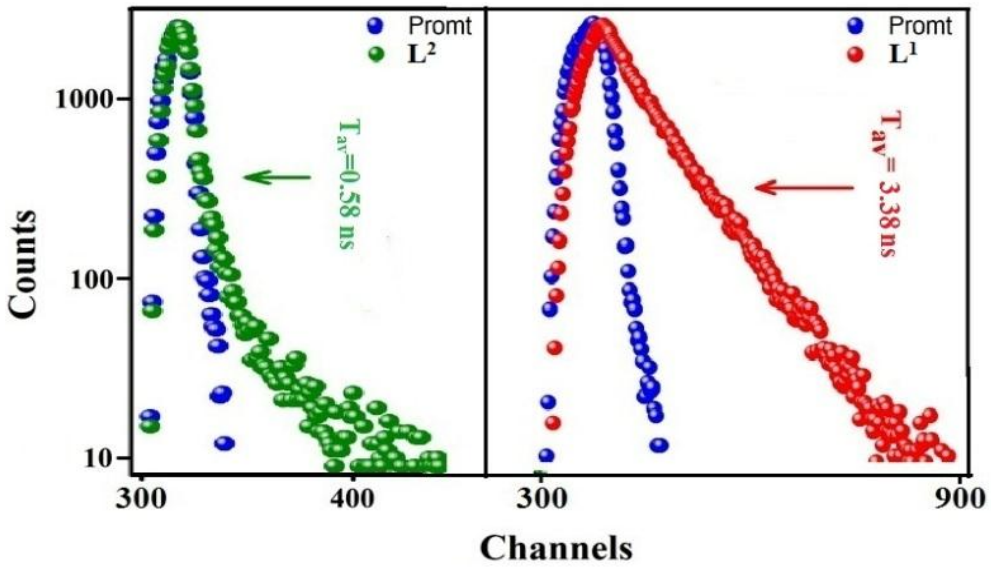

Fig. S26 Life time comparison of L^1 and L^2 at 440 nm (excitation at 340 nm)

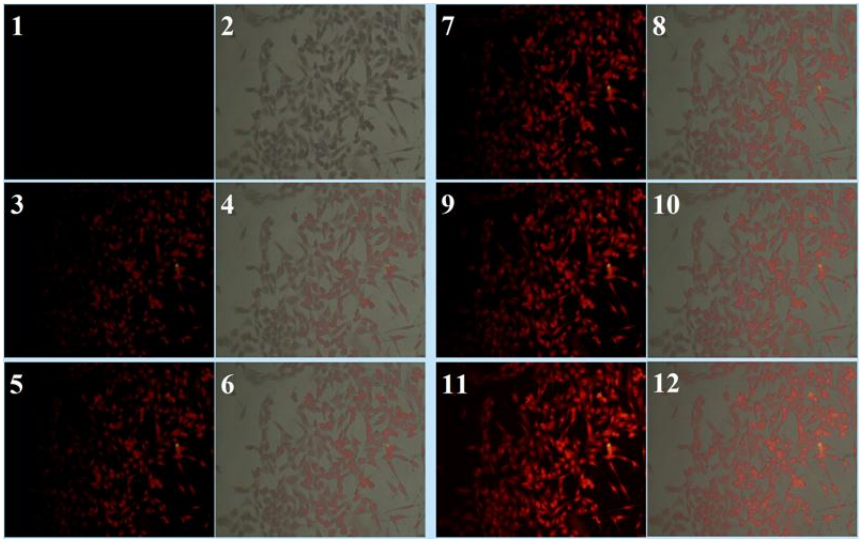

Fig. S27 Phase contrast; fluorescence, and ratio image of HeLa cells after incubation with (1, 2) 0 μM; (3, 4) 2 μM; (5, 6) 4 μM; (7, 8) 6 μM; (9, 10) 8 μM; (11, 12) 10 μM Hg^{2+} with $\mathbf{L^1}$ for 30 min at 25 °C respectively and the samples were excited at ~550 nm.

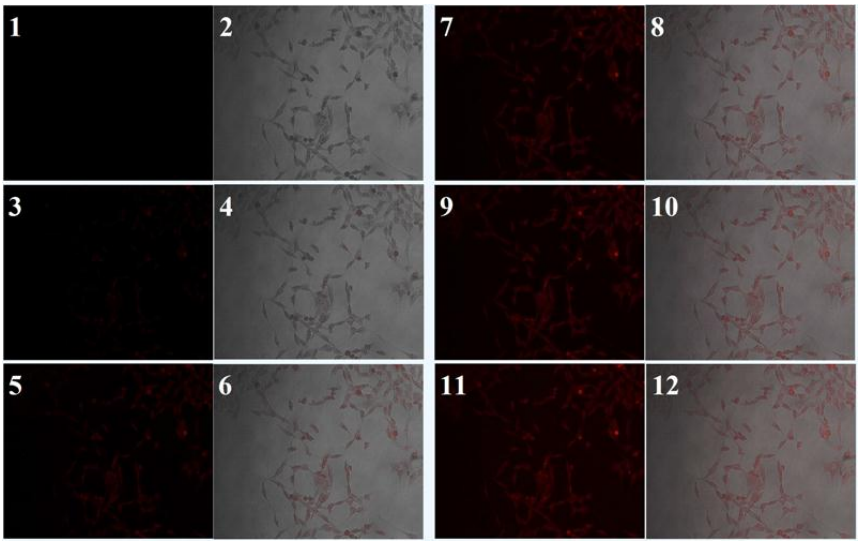

Fig. S28 Phase contrast; fluorescence, and ratio image of HeLa cells after incubation with (1, 2) 0 μM; (3, 4) 2 μM; (5, 6) 4 μM; (7, 8) 6 μM; (9, 10) 8 μM; (11, 12) 10 μM Hg^{2+} with $\mathbf{L^2}$ for 30 min at 25 °C respectively and the samples were excited at ~550 nm.

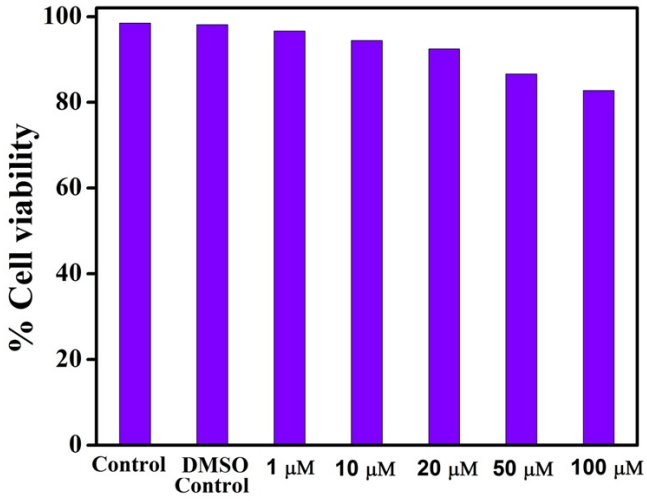

Fig. S29 Cytotoxic effect of $\mathbf{L^1}$ (1, 10, 20, 50 and 100 μM) in HeLa cells incubated for 6 h.

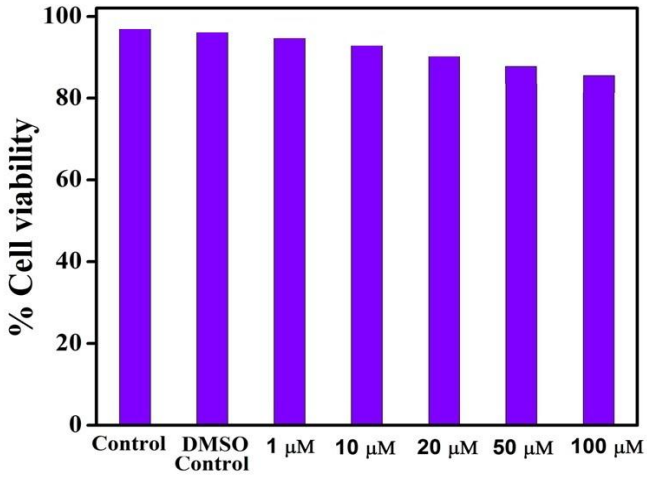

Fig. S30 Cytotoxic effect of $\mathbf{L^2}$ (1, 10, 20, 50 and 100 μM) in HeLa cells incubated for 6 h

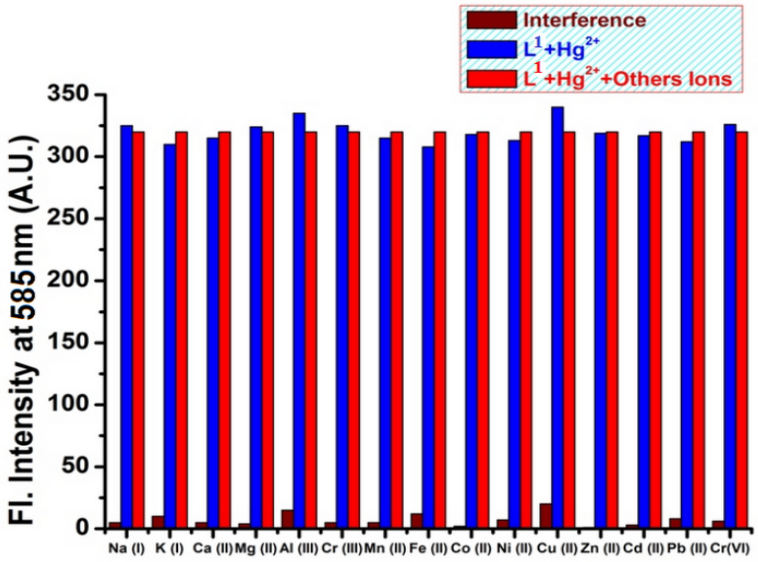

Fig. S31 Change of relative fluorescence intensity profile of $\mathbf{L^1}$ in presence of different metal ions in HEPES buffer (1 mM, pH 7.4; DMSO/water: 1/9, v/v) at 25 °C (λ_{ex} = 340 nm).

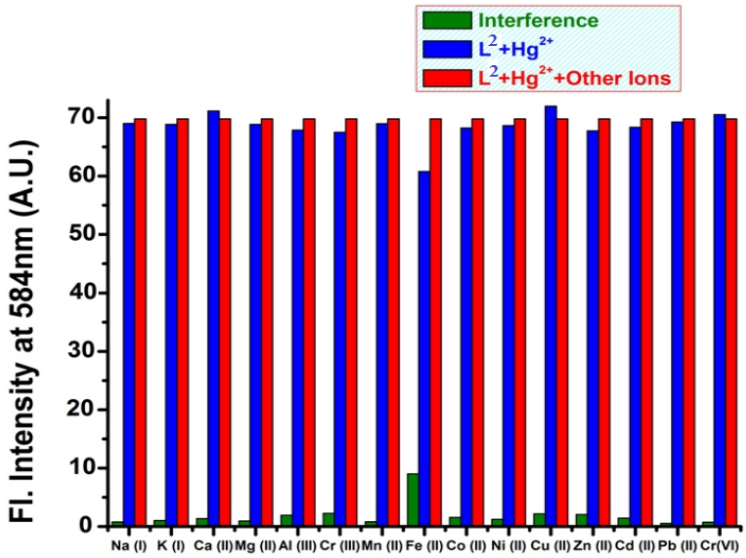

Fig. S32 Change of relative fluorescence intensity profile of $\mathbf{L^2}$ in presence of different metal ions in HEPES buffer (1 mM, pH 7.4; DMSO/water: 1/9, v/v) at 25 °C (λ_{ex} = 555 nm).

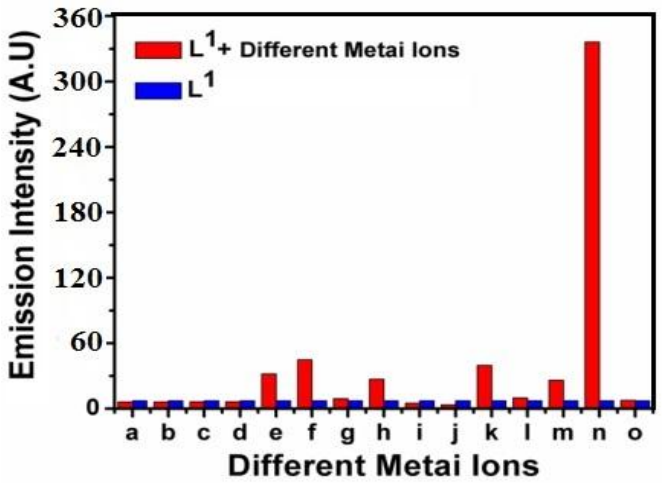

Fig. S33 Fluorescence intensity assay of $\mathbf{L^1}$ in presence of different metal ions in HEPES buffer (1 mM, pH 7.4; DMSO/water: 1/9, v/v) at 25 °C (λ_{ex} = 340 nm), (a) Na^+, (b) K^+, (c) Ca^{2+}, (d) Mg^{2+}, (e) Al^{3+}, (f) Cr^{3+}, (g) Mn^{2+}, (h) Fe^{3+}, (i) Co^{2+}, (j) Ni^{2+}, (k) Cu^{2+}, (l) Zn^{2+}, (m) Cd^{2+}, (n) Hg^{2+} and (o) Pb^{2+}

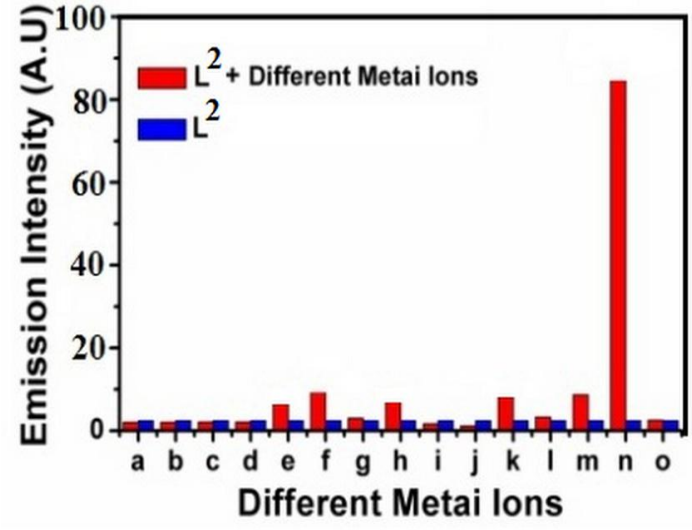

Fig. S34 Fluorescence intensity assay of $\mathbf{L^2}$ in presence of different metal ions in HEPES buffer (1 mM, pH 7.4; DMSO/water: 1/9, v/v) at 25 °C (λ_{ex} = 555 nm), (a) Na^+, (b) K^+, (c) Ca^{2+}, (d) Mg^{2+}, (e) Al^{3+}, (f) Cr^{3+}, (g) Mn^{2+}, (h) Fe^{3+}, (i) Co^{2+}, (j) Ni^{2+}, (k) Cu^{2+}, (l) Zn^{2+}, (m) Cd^{2+}, (n) Hg^{2+} and (o) Pb^{2+}.

Fig. S35 Visual color change of (a) $\mathbf{L^1}$ and (b) $\mathbf{L^2}$ with increase of concentration of Hg^{2+} ions added (0-30 µM) in HEPES buffer (1 mM, pH 7.4; DMSO/water: 1/9, v/v) at 25 °C.

Fig. S36 Fluorescence color change of (a) $\mathbf{L^1}$ and (b) $\mathbf{L^2}$ with increase of concentration of Hg^{2+} ions added (0-30 µM) in HEPES buffer (1 mM, pH 7.4; DMSO/water: 1/9, v/v) at 25 °C.

Table S1 Crystal data and details of refinements for **L**[1] and **L**[2]

Empirical Formula	$C_{36}H_{38}N_4O_3$	$C_{35}\ H_{35}\ N_5\ O_4$
Formula Weight	574.70	589.68
Crystal system	Monoclinic	Orthorhombic
Space group	P 21/n	P na21'
a (Å)	16.391(2)	9.1305(6)
b (Å)	11.840(16)	16.6442(12)
c (Å)	17.229(2)	20.2034(13)
α	90°	90°
β	111.15°(10)	90°
γ	90°	90°
Volume ($Å^3$)	3118.6(7)	3070.3(4)
Temperature (K)	293(2)	293(2)
Z	4	4
ρ_{calc} (g/cm^3)	1.224	1.276
μ (mm^{-1})	0.079	0.085
F(000)	1224	1248
θ range (deg)	2.26-26.90	2.45-26.02
Reflections collected / unique	6644/2384	5844/1959
R indices (all data)	0.0665	0.0610
Goodness-of-fit on F^2	0.982	0.918

Table S2A Selected bond distances (Å) for **L^1** and **L^2**

Bond distances (Å)			
L^1		**L^2**	
O_1- C_1	1.225(4)	O_1- C_1	1.212(7)
C_1- C_2	1.462(5)	C_1- C_2	1.474(9)
N_1 -C_1	1.369(4)	N_1 -C_1	1.381(8)
N_1- N_2	1.419(4)	N_1- N_2	1.382(6)
N_1- C_8	1.500(4)	N_1- C_8	1.496(7)
C_2 -C_7	1.384(4)	C_2 -C_7	1.368(8)
C_7- C_8	1.525(4)	C_7- C_8	1.532(8)
N_2- C_{29}	1.246(4)	N_2- C_{29}	1.271(6)
C_{29}- C_{30}	1.479(5)	C_{29}- C_{30}	1.450(8)
N_3 -C_{12}	1.376(4)	N_3 -C_{12}	1.397(7)
N_4- C_{17}	1.391(4)	N_4- C_{17}	1.397(7)
C_8- C_9	1.506(4)	C_8- C_9	1.494(8)
C_8 -C_{20}	1.504(4)	C_8 -C_{20}	1.528(7)
C_{10} -C_{11}	1.367(4)	C_{10} -C_{11}	1.376(8)
C_{13}- C_{14}	1.380(4)	C_{13}- C_{14}	1.388(8)
C_{15}- C_{16}	1.391(4)	C_{15}- C_{16}	1.378(7)
C_{18}- C_{19}	1.366(4)	C_{18}- C_{19}	1.369(8)
O_3 -C_{33}	1.370(4)	O_3- N_5	1.217(7)
O_3- C_{36}	1.436(5)	O_4- N_5	1.231(7)

Table S2B Selected bond angles (°) for **L^1** and **L^2**

Bond angles (°)			
L^1		**L^2**	
O_1- C_1- N_1	126.5 (4)	O_1- C_1- N_1	126.6 (7)
O_1- C_1- C_2	127.8 (3)	O_1- C_1- C_2	127.9 (7)
N_1 -C_1- C_2	105.7 (3)	N_1 -C_1- C_2	105.5 (7)
C_1 -N_1- N_2	130.9 (3)	C_1 -N_1- N_2	128.7 (5)
C_1- N_1 -C_8	114.8 (3)	C_1- N_1 -C_8	114.4 (6)
N_2- N_1 -C_8	114.0 (3)	N_2- N_1 -C_8	116.8 (5)
C_{29}- N_2- N_1	117.1 (3)	C_{29}- N_2- N_1	118.7 (5)
C_{14}- O_2 -C_{15}	118.4 (2)	C_{14}- O_2 -C_{15}	117.3 (5)
C_{33}- O_3- C_{36}	118.3 (4)	O_3- N_5- O_4	123.9 (8)
C_{12}- N_3 -C_{23}	121.6 (3)	C_{12}- N_3 -C_{23}	122.1 (5)
C_{12} -N_3- C_{21}	122.3 (3)	C_{12} -N_3- C_{21}	121.6 (5)
C_{23}- N_3 -C_{21}	116.1 (3)	C_{23}- N_3 -C_{21}	116.2 (6)
C_{17}- N_4- C_{27}	119.3 (3)	C_{17}- N_4- C_{27}	121.9 (7)
C_{17}- N_4- C_{25}	120.2 (3)	C_{17}- N_4- C_{25}	118.4 (7)
C_{27}- N_4 -C_{25}	117.1 (3)	C_{27}- N_4 -C_{25}	119.0 (6)
N_1- C_8 -C_7	98.8 (2)	N_1- C_8 -C_7	99.2 (5)
C_{20}- C_8- C_7	112.8 (3)	C_{20}- C_8- C_7	109.6 (5)

Table S3A Life time detail of **L^1** at 440 nm

	B_1	B_2	T_1(ns)	T_2(ns)	T_{av}(ns)	X^2	φ	K_r	K_{nr}
Ligand (L^1)	69.02	30.98	2.07	3.98	3.38	1.012	0.30	0.09	0.21
L^1+Hg (1:0.5)	82.99	17.01	2.26	6.61	3.01	1.018	0.24	0.08	0.25
L^1+Hg (1:1)	86.50	13.50	1.18	5.27	1.99	1.024	0.09	0.04	0.46

Table S3B Life time detail of **L^1** at 585 nm

	T (ns)	X^2	φ	K_r	K_{nr}
Ligand (L^1)	1.58	1.014	0.14	0.08	0.55
L^1+Hg (1:1)	2.12	1.034	0.98	0.46	0.011

Table S4. Life time detail of **L^2** at 584 nm

	B_1	B_2	T_1(ns)	T_2(ns)	T_{av}(ns)	X^2	φ	K_r	K_{nr}
Ligand (**L^2**)	53.63	46.37	0.19	1.85	0.95	1.012	0.14	0.15	0.90
L^2+Hg (1:0.5)	8.22	91.78	0.39	1.72	1.61	1.001	0.43	0.27	0.35
L^2+Hg (1:1)	2.57	97.43	0.86	1.84	1.82	1.054	0.68	0.37	0.17

Table S5. Selectivity coefficient (k_{sc}) for Hg^{2+} over competitive cations

Interfering metal ions	Selectivity coefficient (k_{sc}) of **L**[1]	Selectivity coefficient (k_{sc}) of **L**[2]
Na^+	700	698
K^+	720	730
Mg^{2+}	740	702
Ca^{2+}	760	650
Cr^{3+}	100	103
Fe^{3+}	126	134
Co^{2+}	352	311
Ni^{2+}	440	382
Zn^{2+}	196	208
Cu^{2+}	88	80
Cd^{2+}	128	97
Al^{3+}	114	61
Pb^{2+}	509	101
Mn^{2+}	352	91

Selectivity coefficient (k) was calculated as $k_{B,A} = m_B/m_A$; where m_B = d/dc(signal of B) and m_A = d/dc(signal of A); dc = change of concentration of species; B = Hg^{2+} (10 μM) and A = other interfering metal ion (10^{-4} M).